

Thermal-equilibrium processes in amorphous silicon

R. A. Street, J. Kakalios, C. C. Tsai, and T. M. Hayes

Xerox Corporation, Palo Alto Research Center, Palo Alto, California 94304

(Received 31 July 1986)

Data are presented which show that a major part of the localized electronic state distribution in hydrogenated amorphous silicon is in thermal equilibrium at elevated temperatures. Measurements of electronic transport are reported, with particular emphasis on the effects of annealing and cooling the samples. Two regimes of behavior are observed. When samples are cooled below a temperature T_E , the electronic and atomic structures slowly relax with a temperature-dependent time constant. In *n*-type samples the relaxation time is several weeks at room temperature, and T_E is $\sim 130^\circ\text{C}$. In *p*-type samples the time constant is a few hours and T_E is $\sim 80^\circ\text{C}$. The second regime above T_E corresponds to a relaxation time short compared to experimental times, and the structure attains a metastable thermal equilibrium. We show that the defect-compensation model of doping provides an accurate phenomenological description of the results. Furthermore, a quantitative fit to the data is obtained using the known density-of-states distribution. The bonding rearrangements that enable changes in the localized-state structure are discussed. We propose that the motion of bonded hydrogen is important, and that it can be considered to form a separate substructure that has properties similar to a glass. In this model the equilibration temperature T_E is identified with the glass transition temperature. New measurements of hydrogen diffusion are presented to support the model.

I. INTRODUCTION

Ever since the initial studies of amorphous semiconductors, these materials have been divided into two categories.¹ One group comprises the glasses, of which As_2Se_3 and Se are well-studied examples. Glasses have the property of being formed by cooling from the melt. During cooling the viscosity increases eventually to the point that structural changes are too slow to follow the cooling rate. The glass transition reflects the transition from a structure which is in metastable thermal equilibrium to one in which there is a frozen-in nonequilibrium state, from which slow relaxation can occur. The glass transition is kinetically determined, and occurs at a temperature that depends on the cooling rate of the glass. To a large measure, the electronic properties of these glasses are defined by the metastable thermal equilibrium of the structure at the glass transition temperature. Thus it is generally found that a glass will always exhibit the same electronic properties independent of the preparation method, with only minor differences depending on the details of annealing and cooling.

The second group is the "amorphous" materials, of which Si and Ge are the best known examples. These materials cannot be made amorphous by cooling from the melt, and instead are typically deposited by evaporation, sputtering, or plasma decomposition. The general view of such deposition processes is that the resulting material will be far from thermal equilibrium. Instead, the structure will be solely determined by the way that the growing surface takes up the impinging atoms and forms a bonded network. Therefore, in contrast to the glasses, the electronic properties are expected to vary strongly from sample to sample, depending on the details of the deposition.

In amorphous silicon such behavior is indeed observed.

Evaporated *a*-Si contains about 10^{19} cm^{-3} dangling-bond defects.² The defect density is reduced to about 10^{15} cm^{-3} in the best hydrogenated glow-discharge samples.³ However, the glow-discharge technique can also produce high defect densities and visible columnar microstructure, depending on the details of the deposition.⁴

On the other hand, the electronic properties of *a*-Si:H are not completely determined by the deposition process. For example, there are thermally induced changes of the material. Samples deposited at low temperature (e.g., 100°C) have a high defect density, which is reduced by annealing to 250°C .⁵ In a similar manner, defects introduced by an extrinsic process, such as prolonged illumination, can also be removed by annealing.^{6,7} However, the description of these processes in terms of thermal equilibrium can be applied only in a very restricted sense. Annealing must presumably change the structure in a way that approaches the equilibrium state. However, the annealing may apply to only a very small subset of structural configurations, for example, defects created by illumination, and it is unclear whether even this subset reaches equilibrium.

Since it is generally accepted that the equilibrium state of any material is a crystalline form, no amorphous material is in complete equilibrium. The issue, therefore, is the extent to which equilibrium processes determine the structure and properties of a particular material. In glasses, the equilibration is extensive, encompassing the local bonding structure. It is only the long-range order that is inhibited from reaching its equilibrium state. The most obvious observable properties associated with the glassy equilibrium are chemical ordering as observed in As_2Se_3 , for example,⁸ and the fact that defect densities are determined by the annealing process alone.⁹

The idea that equilibrium processes are important in *a*-

Si:H was in fact suggested a few years ago in connection with the doping mechanism. In 1982, we introduced a model of defect compensation to account for the observed increase in the dangling bond density with doping concentration.^{10–12} It was proposed that in doped *a*-Si:H, phosphorus (or boron) could be incorporated into the growing film in either three-fold or four-fold coordination. However, the four-fold state is only stable when ionized, and is accompanied by an approximately equal density of dangling bonds, according to the proposed reaction



where D^- represents a negative dangling bond. The subscripts give the coordination and the superscripts the charge of the atom. If this reaction occurs in thermal equilibrium, then by the law of mass action, the concentrations of donors and dangling bonds are given by

$$[P_4^+] = [D^-] \propto [P]^{1/2}. \quad (2)$$

The square-root dependence is indeed observed for both boron and phosphorous doping.¹³ It was therefore deduced that a metastable thermal equilibrium exists at the growing surface. One explanation for this situation was that the surface is less constrained by bonding than the bulk, so that equilibrium is more easily achieved. This doping model is central to the present experiments and is discussed in more detail in Sec. III.

This paper describes experimental evidence that thermal equilibrium processes are much more prevalent in *a*-Si:H than was previously supposed. A brief first report of our results is published elsewhere.¹⁴ We focus on doped *a*-Si:H and show that the electronic states that control the conductivity are in equilibrium above about 100°C. Below this temperature the structure becomes frozen. We discuss the equilibration mechanism, particularly addressing the question of how extensive is the equilibration. Section II describes the experimental results of sweep-out, conductivity, ESR, and other measurements all of which demonstrate the equilibration. Section III describes the mechanisms of equilibration, and Sec. IV discusses our results in relation to other published models and experimental data, in particular, the recent proposals that dangling bonds in undoped *a*-Si:H are also in equilibrium, at least in low-defect-density material.^{15–17} Muller *et al.*¹⁸ have also discussed some ideas of thermal equilibrium based on an analysis of the defect compensation model.

II. EXPERIMENTAL RESULTS

The main experimental observations concern the electronic states of doped *a*-Si:H, as measured by sweep out, dc conductivity, ESR, and luminescence. In particular, we are interested in the changes in the localized state distribution and electron occupancy upon annealing and cooling the samples. Figure 1 shows a schematic density of states diagram for the upper half of the gap in *n*-type material, based on many previous experiments.¹² A quantitative distribution of states is introduced later. Near the middle of the gap are the dangling bond states, negatively charged in *n*-type material, and denoted D^- . The

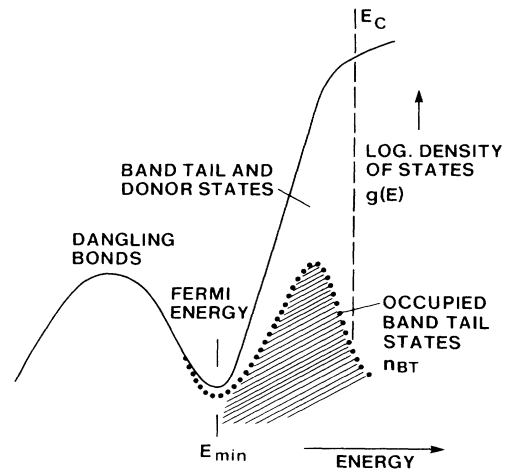


FIG. 1. Schematic density-of-states diagram for *n*-type *a*-Si:H showing the dangling bond band separated from the band tail. The shaded region indicates the electron occupancy of the band tail at some elevated temperature.

conduction-band-tail states below the mobility edge, E_c , are localized and include the donor levels. Deep-level transient-spectroscopy (DLTS) data have found that the band tail and the D^- states are separated by a deep minimum in the density of states at E_{min} about 0.3–0.4 eV below E_c .¹⁹ Therefore, the electron distribution can be divided into those states above or below the minimum. The upper states we denote n_{BT} , and are the focus of several of our measurements.

A. Sample preparation and annealing procedures

Samples of *a*-Si:H are prepared by plasma decomposition of SiH_4 in a glow-discharge deposition system described earlier. The deposition temperature of 230°C and rf power of 2 W were chosen to give the best electronic properties.³ Doping with phosphorus (using PH_3 gas), boron (B_2H_6), and arsenic (AsH_3) is studied at gas-phase concentrations ranging from 10^{-6} to 10^{-2} mole fraction. The sample measurement configurations are different for each experiment and are described below. Annealing was performed both in air and in vacuum, with no differences being observed. Generally, the fastest quench rates were in air. In this case the rate had to be estimated, and is accurate only to a factor 2. In one case quenching in water was used, which gives a significantly higher cooling rate. The slower quench rates were performed by controlled cooling with more accurate rates. The results do not depend on a precise knowledge of the cooling rates.

B. Sweep-out measurements

The sweep-out technique was developed to measure the density of occupied shallow states in doped *a*-Si:H.^{20,21} The samples consist of a thin doped layer imbedded in undoped material, as indicated in Fig. 2. When a bias is applied, the shallow electrons in the doped layer are swept across the thick undoped layer, and are recorded as a current transient. The total charge collected $Q = \int Idt$,

where I is the current, together with the volume \mathcal{V} of the doped layer, give the density of shallow states

$$n_{BT} = Q/\mathcal{V}. \quad (3)$$

Figure 2 shows examples of sweep out data for an n -type sample, and is typical of all the results. The current drops by several orders of magnitude at a time of about 10^{-6} sec. The fact that there is no significant current at a time t means that the density of states has dropped to a very low value at the corresponding energy E_t , where

$$E_t = kT \ln(\omega_0 t). \quad (4)$$

For the present experiments, we use $\omega_0 = 10^{12}$ sec $^{-1}$ and $t = 10^{-6}$ sec, at room temperature, so that E_t is about 0.35 eV. This energy is consistent with the known position of the minimum in the density of states (see Fig. 1), showing that the sweep-out experiment therefore selectively measures only the electrons in band-tail states above the minimum, and is a well-defined quantity.

The experimental details of the measurement are described elsewhere.^{20,21} The results are corrected for the displacement current of the geometrical capacitance, which is minimized by having a thick undoped layer and amounts to about 10% of the measured Q . The thickness of the doped layer is chosen so that depletion effects are not significant. The measured values of Q are typically reproducible to an accuracy of 1–2% or better in n -type samples, and we believe that the absolute value of n_{BT} is accurate to 10–20%. The largest uncertainty is in the exact thickness of the doped layer, which was taken from the deposition rates rather than by direct measurement. Related transient voltage experiments using thick doped layers confirm the densities of n_{BT} ,²² as does ESR data.²³

One advantage of the sweep-out measurement is that the doped layer being studied is sandwiched within a sample that is also covered with an evaporated metal contact.

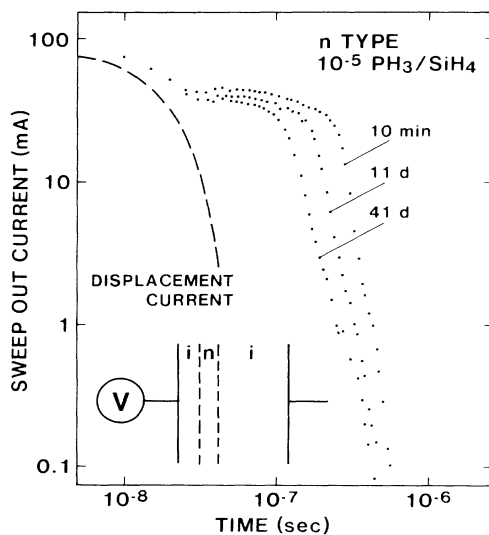


FIG. 2. Examples of sweep-out current pulses for n -type samples at different times after annealing. The displacement current of the geometrical capacitance is indicated by the dashed line. The sample structure is also shown schematically.

Therefore there is no possibility of the results being influenced by the ambient during annealing in air.

Figure 2 compares the sweep-out data for a sample measured at room temperature immediately after annealing to 220°C, and after the same sample has been stored in the dark at room temperature for many days. The density n_{BT} is found to decrease by more than a factor of 2 over this period. The lower n_{BT} values are reflected in a shorter time to sweep out the shallow electrons. Note that the fact that the sweep-out time decreases does not directly imply a change in the energy distribution. The time dependence of the sweep-out is strongly influenced by the carrier transit time and space-charge effects.²¹

In Fig. 3, the decay of n_{BT} over a two month period for n -type samples (As and P doped) with gas-phase doping levels of 10^{-5} – 10^{-2} is shown. In each case the decay has roughly the same shape, and so is evidently independent of the doping level. The decay is nonexponential and approximates to a power law with a time dependence $t^{-0.1}$. Over the first few days, the slope corresponds to a decay time of 10 days, increasing to 200 days later in the decay. It is clear that n_{BT} continues to decay even after two months. We have not been able to determine when, if ever, a steady state is reached.

The decay of n_{BT} is temperature dependent becoming slower at lower temperatures, as is indicated in Fig. 3 (\times data points). More extensive data obtained from conductivity measurements are described in Sec. IID. The lowest temperature investigated is -10°C , when the decay is so slow that only a 10% reduction in n_{BT} is observed in a month.

Similar effects are observed in p -type samples. Examples of sweep-out measurements in boron-doped a -Si:H are shown in Fig. 4. The sweep-out time is much longer than in n -type samples, partly because the Fermi energy is further from the mobility edge and partly because the transit time across the undoped layer is larger. The time-

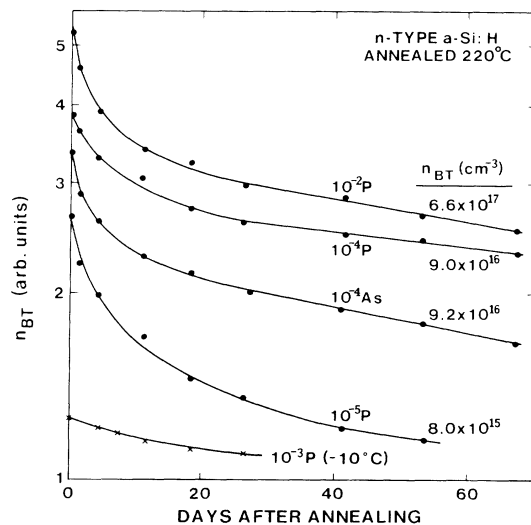


FIG. 3. The time decay of the density of shallow electrons, n_{BT} , after annealing at 220°C, for samples doped with P and As. The decay is at room temperature, except where indicated. The values of n_{BT} at the end of the decay are shown.

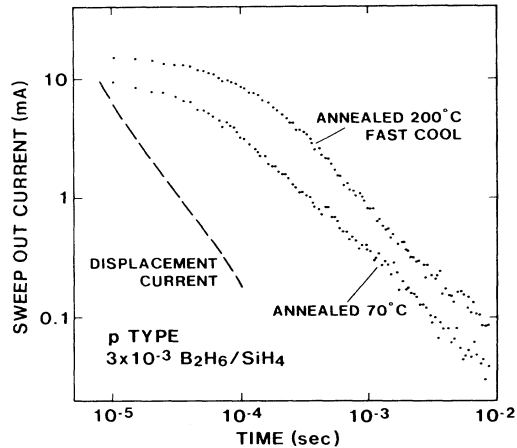


FIG. 4. Examples of the sweep-out current pulses for p -type samples for different annealing temperatures. The displacement current of the geometrical capacitance is indicated by the dashed line.

dependent decrease in the sweep-out current is also more gradual. All three effects occur primarily because the valence-band tail is broader than the conduction-band tail. Application of Eq. (4) indicates that the shallow states extend to a depth of about 0.5 eV. The slow decrease in current with time increases the uncertainty in the measurement of Q , although n_{BT} remains a well-defined reproducible quantity. The time integral is continued until the current approaches the background noise, and the typical measurement uncertainty is $\sim 5\%$. In Fig. 4 we show that n_{BT} is smaller for samples annealed at a lower temperature and further data on this aspect of the results for n - and p -type samples are described shortly. Figure 5 gives an example of the room-temperature decay of n_{BT} for p -type a -Si:H after annealing. We observe that the decay is faster than in n -type samples, approaching a steady state in only a few hours at room temperature.

Thus we have demonstrated a slow relaxation of n_{BT} in both n - and p -type a -Si:H after annealing. This result is confirmed by the other experiments described in later sections.

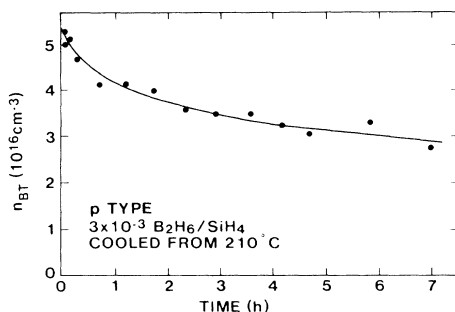


FIG. 5. An example of the room-temperature time decay of shallow holes in p -type a -Si:H after annealing at 210°C . The sample was quenched in cold water.

We next show that the values of n_{BT} are sensitive to the details of the annealing process, as indicated in the data for n -type samples in Fig. 6. In each of these measurements, the sample is annealed to the indicated temperature, then cooled to room temperature and measured within a few minutes. Hence the slow decay process has not had time to influence the results. There are various aspects of the data to discuss. At annealing temperatures above about 130°C , the quenched in value of n_{BT} increases by up to a factor of 2, providing that the quench rate is rapid. Above 200°C , no further increase in n_{BT} is observed. The values of n_{BT} are independent of the annealing time (10 min for the data shown), and also are independent of which order the annealing temperature is chosen. Thus n_{BT} is not influenced by the prior sample history and n_{BT} evidently attains a steady-state value during the anneal. However, the results are very sensitive to the cooling rate, so that samples that are cooled slowly show a much weaker annealing temperature dependence.

At annealing temperatures below 130°C , the properties are different. A dependence on the annealing time is found, such that longer times result in lower values of n_{BT} . The data show a significant reduction in n_{BT} when the annealing time is increased from 10 min to 1 h. We have already seen that such a reduction also occurs at room temperature, but on a very much longer time scale. In addition, the results are no longer independent of sample history. For the data of Fig. 5, the 10-min anneals were performed at progressively lower temperatures, and then the 1-h anneals were made, also starting at the higher temperatures. If a sample is annealed at 80°C for 1 h, for example, a subsequent 10-min anneal would not restore the higher value of n_{BT} . Additional anneals would, in fact, decrease n_{BT} further. Thus the low-temperature properties are characterized by relaxation of n_{BT} rather than a steady-state value.

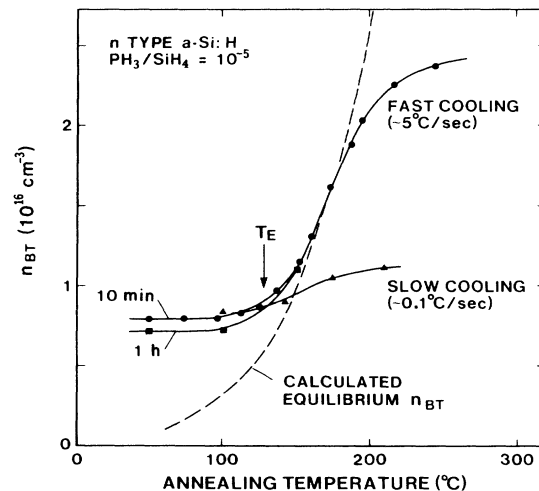


FIG. 6. Values of n_{BT} in n -type a -Si:H measured at room temperature after annealing and cooling at different rates. The annealing times are shown. The dashed line is calculated as described in the text.

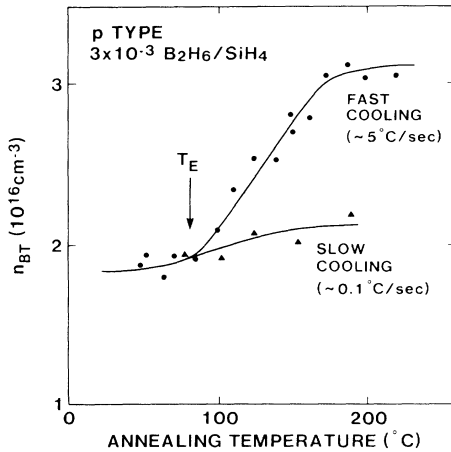


FIG. 7. Data for holes in *p*-type *a*-Si:H similar to that shown in Fig. 6. Note the lower value of the equilibration temperature T_E .

p-type samples show qualitatively the same annealing properties, as indicated by the data in Fig. 7. As before, n_{BT} is increased by annealing to higher temperatures, and slow cooling reduces this effect. The temperature below which n_{BT} departs from its steady-state value is about 80°C, compared to 130°C in *n*-type samples.

C. Interpretation of annealing experiments

The annealing experiments are of central importance to this work, since they establish that thermal equilibrium occurs. We therefore discuss their interpretation before describing the remainder of the experimental information.

The data in Fig. 6 has two regions of behavior, corresponding to the high-temperature region above $\sim 130^\circ\text{C}$ and the low-temperature region below. The transition temperature is referred to as T_E . *p*-type samples show the same properties except for a lower T_E . In the low-temperature region below T_E , n_{BT} relaxes slowly compared to the experimental time scale (e.g., the anneal time of 10 min). It has already been shown that at room temperature the relaxation time is of order weeks for *n*-type *a*-Si:H, and decreases still further at lower temperature. Thus below T_E the data are described by a thermally activated relaxation from an initial value of n_{BT} .

On the other hand, the n_{BT} data above T_E is characteristic of a steady state since there is no longer any dependence on the annealing time. Furthermore, the steady-state value increases with temperature. Evidently the reason that a steady state is reached is that at the elevated temperature, the relaxation time decreases, and becomes less than the experimental time scale. Thus n_{BT} is free to reach a steady-state value determined by thermally controlled interactions among the set of states that determine n_{BT} . Hence a thermal equilibrium is established within these states. The relaxation time observed at temperatures below T_E can therefore be equated with the equilibration time, which we denote $\tau_E(T)$.

The fact that the equilibration time is short above T_E is manifest in the cooling rate dependence. Equilibrium will

be maintained as long as the equilibration can keep up with the cooling rate. As cooling proceeds, $\tau_E(T)$ increases and eventually equilibrium cannot be maintained; instead the structure freezes, and passes into the low-temperature region. It is clear that the freezing temperature will be higher for fast cooling than for slow cooling. The data of Fig. 6 show the frozen-in values. For temperatures between 130°C and 200°C, fast quenching freezes in the equilibrium value of n_{BT} at those temperatures. Above 200°C, τ_E is so small that equilibrium is maintained even with rapid cooling down to about 200°C. On the other hand, equilibrium persists down to $\sim 150^\circ\text{C}$ with slow cooling, so that the frozen-in values are correspondingly lower. Exactly the same arguments apply to *p*-type samples apart from the different temperatures at which these effects occur.

Confirmation that the frozen-in values of n_{BT} at high annealing temperatures are limited by the cooling rates, has been obtained in one case. In the *p*-type sample shown in Fig. 7, n_{BT} saturates at about $3 \times 10^{16} \text{ cm}^{-3}$ above 190°C for fast quenching in air. The data in Fig. 5 show the decay of the same sample, annealed at 210°C, but quenched in cold water. The much higher cooling rate results in an initial value of n_{BT} , which is nearly twice as large ($5 \times 10^{16} \text{ cm}^{-3}$).

The experimental data provide values for $\tau_E(T)$. At temperatures below T_E , the relaxation time can be measured directly as in Fig. 3. Since the decay is nonexponential, we arbitrarily define τ_E as the time at which n_{BT} has decreased to 60% of its initial value. For the lowest-temperature data we rely on scaling because the time to reach 60% is too long. At T_E the equilibration time is set by the annealing time, and at higher temperatures it is estimated from the cooling rates. These results are shown in Fig. 8 for both *p*- and *n*-type samples, although the data are more extensive for the *n*-type. $\tau_E(T)$ increases from ~ 1 sec at 200°C to about a year at -10°C . There is curvature in the Arrhenius plot, indicating that the activation energy for equilibration increases from about 0.65 eV at low temperature up to 1.0 eV. $\tau_E(T)$ is smaller in *p*-type samples, consistent with the lower equilibration temperature. In Fig. 8 we have included relaxation data from conductivity experiments described in Sec. II D.

To summarize our arguments, we assert that thermal equilibrium requires two features. One is that structural rearrangements can take place, so that within a set of available states the lowest-energy configuration can be found. The second feature is that there is sufficient time to achieve the equilibrium state. Our measurements show that indeed the equilibration time is short compared to the measurement time above T_E . It is perhaps not obvious that variations in n_{BT} represent structural changes. However, according to the doping model for *a*-Si:H, n_{BT} is fixed by the density of donors, N_{donor} , and of dangling bonds N_{DB} , to a good approximation (see Sec. III A) by

$$n_{BT} = N_{\text{donor}} - N_{\text{DB}} \quad (5)$$

Therefore n_{BT} is directly related to the localized state structure. Although Eq. (5) is derived from a specific model, it is also an equation of charge neutrality. It is therefore of general applicability in the sense that a

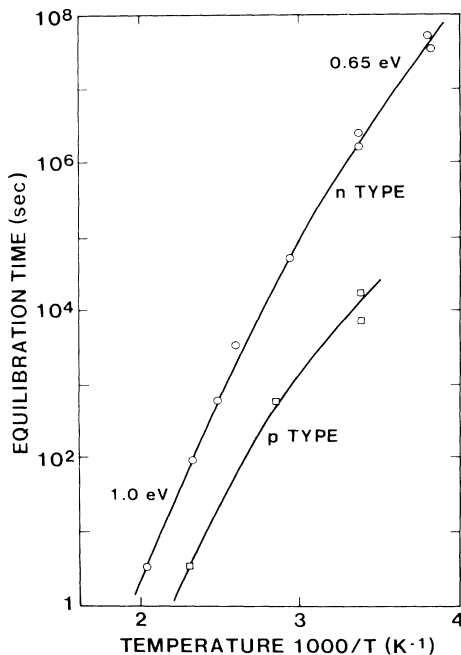


FIG. 8. The temperature dependence of the equilibration time $\tau_E(T)$, for *n*-type and *p*-type samples deduced from sweep out and conductivity experiments.

change in n_{BT} must be accompanied by some change in the density of states to take up the extra charge. We therefore conclude from our observations that the subset of structural states that determine n_{BT} must be in thermal equilibrium. In Sec. III the nature of these states is discussed further.

D. Conductivity experiments

Changes in n_{BT} and any related rearrangement of electronic states must be observed in other measurements, and indeed they are. Some of our results are published separately.²⁴ Figure 9 shows the temperature dependence of the dc conductivity σ for one *n*-type sample, comparing different quenching rates and the effects of relaxation at room temperature for two months. The quenching experiments are performed by cooling the sample from the annealing temperature of 200°C through T_E to room temperature at the indicated rates. At 300 K, the relaxation rates are sufficiently long that further control of the cooling is not necessary. The samples are then cooled further, and the conductivity is measured upon warming slowly (warming rate 2–3 C/min). For the fastest cooling rate, the samples are quenched in air; for all the others, the samples are mounted on a cold finger in vacuum. The heating rate during the measurements is significant only near T_E when the structure starts to equilibrate and the conductivity is time dependent, as will be shown later.

Figure 9 shows that below T_E , the faster quenching rates give a larger dc conductivity. The results are obviously consistent with the sweep-out data since fast quenching gives a larger n_{BT} . Similarly, when the sample is allowed to relax for an extended time, both the conduc-

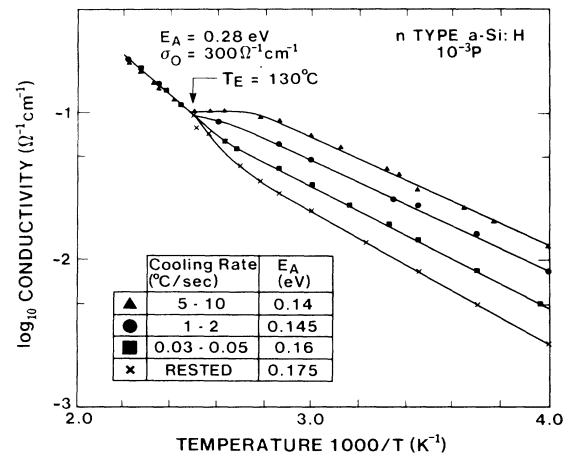


FIG. 9. The temperature dependence of the dc conductivity immediately after annealing when cooled at different rates, and after being stored at room temperature for two months. The activation energies in the low-temperature region are shown.

tivity and n_{BT} decrease. The changes in conductivity arise from an increase in the activation energy, from 0.14 to 0.17 eV. The conductivity prefactor σ_0 is unchanged at a value of $\sim 5 \Omega^{-1} \text{cm}^{-1}$. Hence the variations in n_{BT} correspond to shifts in the Fermi energy, as would be expected.

Above the equilibration temperature, the different conductivity curves converge to a single set of values which are independent of the preceding history. This result is a signature of the equilibration, since all dependence of prior annealing and cooling must by definition disappear. In this region, the activation energy is significantly increased, to 0.28 eV for the doping level shown. Similar results occur at all measured doping levels, as is shown in Fig. 10. In each case, there is a pronounced kink at T_E with a change in the activation energy and prefactor. These results are obtained after fast quenching which gives a larger change of slope at T_E than for slow cooling.

Near T_E , at the transition between the two regions, the conductivity curves depend also on the heating or cooling rates since the relaxation times are similar to the experimental ones. Figure 11 shows examples of data that illustrate that the detailed shape can vary, and that there is hysteresis between heating and cooling. In these experiments the sample is heated and cooled at the same rate, and the cycle can be repeated many times. In the transition region, the conductivity is larger upon cooling than upon heating because the structure is relaxing from a higher temperature equilibrium. The relaxation is shown more clearly in the insert to Fig. 11. In these measurements the warming or cooling is stopped at 400 K to observe the relaxation. It is seen that σ tends toward a constant value midway between the two curves, with a time constant of about 10 min.

The conductivity data also reproduce the annealing and quenching data seen for sweep-out experiments in Figs. 6 and 7. An example of the equivalent conductivity data is given in Fig. 12. As before, all the measurements are at

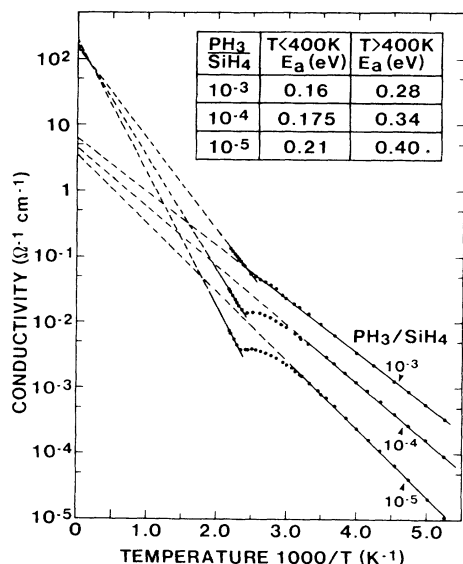


FIG. 10. The temperature dependence of the dc conductivity of n -type samples with different doping levels, after rapid cooling from 200°C. The activation energies of the low- and high-temperature regions are shown, and the dashed lines indicate the extrapolated prefactors.

room temperature and it is found that the conductivity is enhanced by cooling from high temperatures. We observe both the cooling rate dependence for annealing above T_E and the freeze out of the effect below T_E . The close similarity of Figs. 6 and 12 confirms that the measurements are of essentially the same quantity. However, while sweep-out measures all of the shallow electrons, conductivity measures only those carriers, n_{free} , above the mobility edge. Very roughly,

$$n_{\text{free}} = \text{const } n_{\text{BT}} \exp[-(E_C - E_F)/kT]. \quad (6)$$

Hence the conductivity results combine both the changes

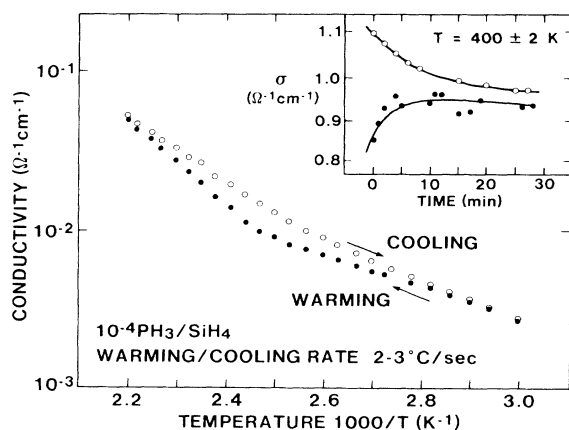


FIG. 11. Measurements of the dc conductivity near T_E showing hysteresis between warming and cooling. The inset shows the slow relaxation to the steady state when the warming or cooling is stopped at 400 K.

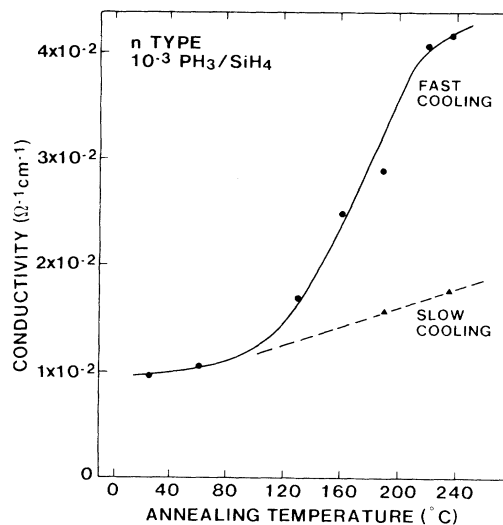


FIG. 12. Values of the dc conductivity measured at room temperature after annealing and cooling at different rates. The results are equivalent to those shown in Figs. 6 and 7.

in n_{BT} and the related shift of E_F . Therefore we expect that the magnitude of the changes in σ will be larger than the equivalent change in n_{BT} , and this can be seen by comparing Figs. 12 and 6.

We also observe slow relaxation of the conductivity below T_E , as was observed for n_{BT} . Figure 13 shows examples of the decay of σ at room temperature, when stored in the dark at different temperatures. The results are fully consistent with those found from sweep out. Again we note that the decays are nonexponential. The data are included in Fig. 8, which gives the temperature dependence of the equilibration time.

Equivalent conductivity measurements have been made on p -type a -Si:H and examples are shown in Fig. 14. As with n -type samples, we observe that below T_E , the conductivity depends on the cooling rates, with fast cooling giving a larger value. Above T_E , the data converge to a single curve. The kink is less clear than in n -type samples, because the activation energies are larger and the change is more gradual. However, the merging of the two sets of data gives a good indication of T_E , which is $\sim 80^\circ\text{--}90^\circ\text{C}$, about 50°C lower than in the n -type samples, and in good agreement with the sweep-out data of Fig. 7.

E. ESR and luminescence measurements

Electron spin resonance provides a third measure of the shallow state density in doped a -Si:H. Previous studies have shown that both neutral donors and electrons (or holes) occupying band-tail states can be observed, and are distinguished by their resonance line shapes.^{25,26} The neutral donors have a strong hyperfine splitting that clearly identifies their origin.²⁶ It has also been confirmed that the total spin density agrees reasonably well with the sweep-out measurement of n_{BT} , except possibly at the highest doping level.^{12,23,27} The density of doubly occu-

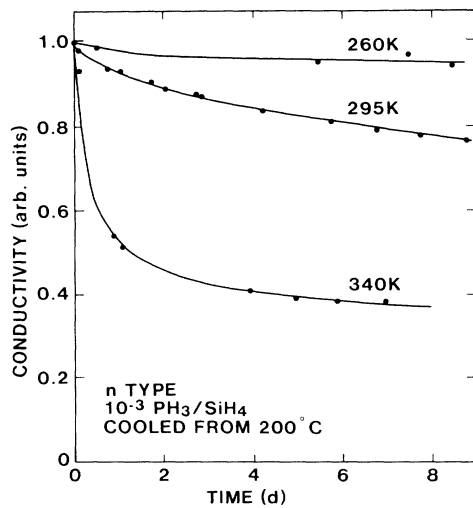


FIG. 13. The time decay of the dc conductivity after annealing at 200°C and cooling to different temperatures. The results show that the decay times are strongly temperature dependent.

pied shallow states must therefore be small. ESR measurements further confirm the annealing and relaxation behavior described in the preceding sections. Figure 15 compares fast-quenched, slow-quenched, and relaxed samples for one phosphorus-doped *n*-type sample (10^{-4} PH_3/SiH_4). The sequence of measurements goes from left to right in Fig. 15, starting with a sample that had been rested at room temperature for about a year. It is seen that the largest spin density occurs after fast quenching, and that slow relaxation at room temperature is observed, both in agreement with the results of the transport measurements. These effects occur for both donors and

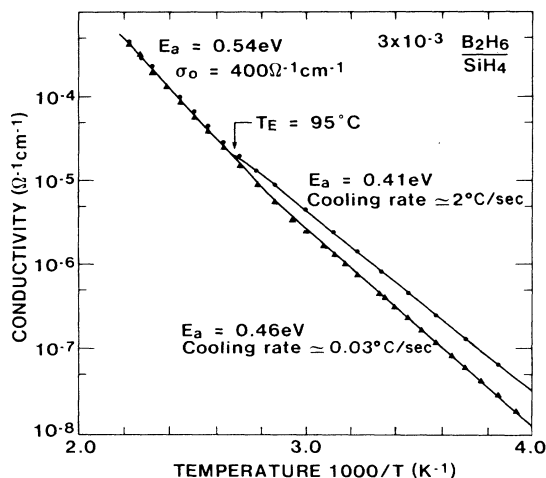


FIG. 14. The temperature dependence of the dc conductivity in *p*-type *a*-Si:H showing the effects of different cooling rates after annealing. The equilibration temperature is indicated where the data merge.

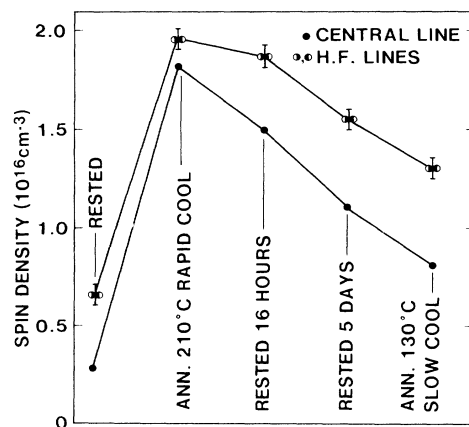


FIG. 15. ESR data on an *n*-type sample with doping level 10^{-4} $[\text{PH}_3]/[\text{SiH}_4]$, showing the spin densities in the central band-tail electron line, and the two hyperfine neutral donors lines. The experiments are performed at 40 K. The measurements show the sequence of changes in spin density upon annealing and resting the sample at room temperature.

band-tail states. The detailed equilibration dependence is different for the donor and band-tail states, but the larger relative effect on the band-tail electrons is consistent with the expected density of states distribution.²⁷

Each experiment so far described measures n_{BT} or a closely related quantity. We have also studied the changes in the dangling bond density using photoluminescence. It is known that the band-edge luminescence at 1.3–1.4 eV is quenched by the dangling bonds introduced by doping, and a lower-energy transition at 0.8–0.9 eV is attributed to radiative recombination at these dangling bonds.²⁸ Figure 16 compares luminescence spectra of a pair of identical *n*-type samples, one of which was fast quenched from 200°C and the other had been left at room temperature for an extended time. The fast-quenched sample has a larger luminescence intensity by about 30%, with a relatively larger intensity in the band-edge line and a lower intensity at 0.8 eV, compared to the sample in the rested state. The results were checked by repeating the experiment five days later with the same pair of samples, except that the “rested” sample was annealed and fast quenched just before the measurement. In this experiment the more recently annealed sample now had the higher intensity, showing that the differences in the initial experiment are not due to permanent differences in the two samples. At a doping level of 10^{-3} , it is known that both luminescence bands decrease in intensity with increasing doping, and the effect is attributed to the increasing dangling bond density.²⁸ From the changes in the spectrum in Fig. 16, we therefore infer that the dangling bond density is reduced by fast quenching. This result is clearly consistent with an increase in n_{BT} , although the luminescence does not provide any indication of changes in the donor density. The results also indicate that the reduction in N_{DB} is 20–30%, based on the previously measured dependence of luminescence on doping level.²⁸

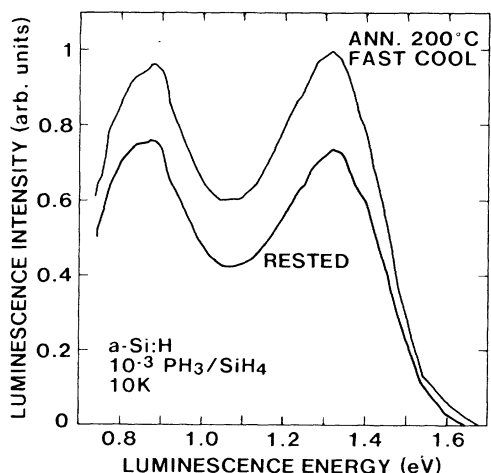


FIG. 16. Luminescence spectra of n -type a -Si:H measured at 10 K, comparing a rested sample and one after annealing and rapid cooling.

F. Bias annealing effects

The experiments described above find that thermal equilibration of the localized state structure influences the electronic properties of a -Si:H. As a corollary, one expects that any externally imposed change in the electronic properties would itself be reflected in a modification of the structure in a way that preserved the equilibrium conditions. For example, if an applied bias causes carrier depletion, then the Fermi energy will move towards the middle of the gap. We show that the equilibrium is altered in the way expected. These results are described in more detail elsewhere²⁹ and are only summarized here.

Figure 17 compares the sweep-out data before and after annealing with an applied bias, for both n - and p -type samples. The annealing temperature is just above T_E in both cases and cooling is fairly slow. Thus, a relatively low value of n_{BT} is quenched in. For bias annealing, a 10-V depletion bias is applied during annealing and subsequent cooling to room temperature. Since the sweep-out sample has only a thin doped layer, we expect the layer to

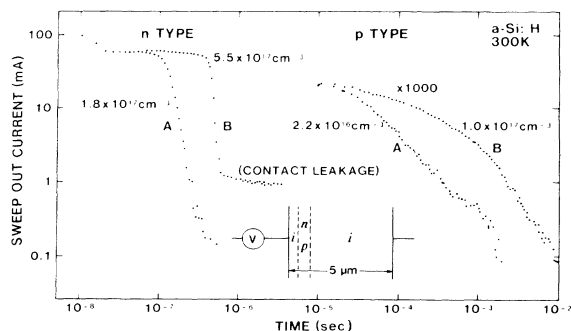


FIG. 17. Sweep-out currents for n -type and p -type a -Si:H using the sample structure as indicated. Curves A are for samples annealed without bias, and B corresponds to a depletion bias during annealing and subsequent cooling.

be approximately uniformly depleted. It is observed that when the bias is removed after cooling, n_{BT} has increased by as much as a factor 3. The excess value relaxes slowly, with a time constant that is the same as is observed for rapid quenching, showing that the same mechanism applies in both experiments. The bias effect can be induced in p -type samples at room temperature as described elsewhere.²⁹ The inducing time is similar to the decay time, being a few hours. We observe no significant room-temperature induction in n -type samples, at least for bias times of a few hours, and interpret its absence as due to the much longer equilibration times. The excess n_{BT} can be removed by annealing, and we find that the annealing temperature is about 50°C lower for p -type samples compared to n type, which agrees well with the difference in T_E .

III. THE EQUILIBRATION PROCESS

The experimental results in Sec. II find that a metastable thermal equilibrium determines the density of n_{BT} , and that the equilibrium density is temperature dependent. A temperature-dependent relaxation time causes the structure to “freeze” below about 100°C. In this section we discuss the equilibration mechanism, and in particular show that it can be explained in terms of the defect compensation model of doping. After first reviewing this model, we show how it relates to the present results, and then discuss possible microscopic mechanisms.

A. The defect compensation model of doping

This model was developed to account for several properties of doped a -Si:H that are not found in its crystalline counterpart, and is described in detail elsewhere.^{10,11,12,27} As the phosphorus or boron concentration is increased, so does the density of dangling bonds.^{28,30,31} These defects are charged, negative in n -type and positive in p -type samples, and their density increases as the square root of the total impurity concentration.¹³ The density of shallow occupied states also increases with the doping level but is only about 10% of the density of N_{DB} . From these results the following is deduced.

- (1) The density of active donors or acceptors approximately equals the density of dangling bonds.
- (2) The majority of donors or acceptors are ionized.
- (3) The donor (or acceptor) density is small compared to the total impurity content $[P]$, and increases as $[P]^{1/2}$.

To account for these results, it was proposed that the following basic reaction occurred during deposition of n -type material:



with a similar reaction for acceptors. The underlying idea is that phosphorus can be either threefold or fourfold coordinated. However, the fourfold state is energetically favorable only if charged, and so is accompanied by a negative compensating dangling bond. A further assumption that metastable thermal equilibrium occurs at the growing surface readily explains the square-root concentration dependences through the law of mass action. Thus the

concept of thermal equilibrium is already introduced into the doping process.

Before applying this model to the problem of equilibration in the bulk, one aspect needs to be clarified. According to the reaction in Eq. (7), only charged donor and dangling bond states are present. Although this is a good approximation to the experimental results, shallow occupied band-tail states are also present, being the quantity n_{BT} , and some of these occupy neutral donor sites, as is evident from the ESR data.²⁶ These states can be understood in terms of the deposition temperature, as follows. The presence of charged states implies that the Fermi energy must be above the D^- band but below the P_4^+ band. In fact, these two bands are relatively well separated by a deep minimum in the density of states, as indicated in Fig. 1, so that there is very little overlap of the two types of states. However, at the high temperature of deposition, typically about 500 K, the Fermi function

$$f(E, E_F, T) = \{1 + \exp[(E - E_F)/kT]\}^{-1}$$

is sufficiently extended in energy that it is impossible to have only P_4^+ and D^- states. The electron density above the minimum E_{min} in the density of states, and the hole (D^0) density below are given by

$$n_{BT} = \int_{E_{min}}^{\infty} g(E) f(E, E_F, T) dE \quad (8)$$

and

$$N_{D^0} = \int_{-\infty}^{E_{min}} g(E) [1 - f(E, E_F, T)] dE. \quad (9)$$

Since, at any finite temperature both quantities cannot be zero, we therefore need to understand which position of E_F best satisfies the model as defined by Eq. (7). We conjecture that it is when E_F is at E_{min} . This position is certainly the correct value in the low-temperature limit. Clearly if E_F is far from E_{min} then there will be a large density of either neutral donors or of neutral dangling bonds, neither of which is allowed by the model nor observed experimentally. As discussed below, our experimental results also indicate that E_F is indeed close to E_{min} . However, this position of E_F does not imply that n_{BT} and N_{D^0} are equal. The density of states $g(E)$ increases much more rapidly above E_{min} than below, because of the asymmetry between the band tail and the defect band (see Fig. 1) so that $N_{D^0} \ll n_{BT}$. Numerical evaluations of N_{D^0} and n_{BT} confirm this result, as described below. Note that N_{D^0} was omitted from the charge neutrality relation, Eq. (5), because it is negligibly small.

In summary, the defect compensation model suggests that the surface is in quasithermal equilibrium during growth and that the Fermi energy is held at the minimum below the band tail by the requirement that the energy is minimized according to the reaction in Eq. (7). The presence of shallow occupied states is then explained by the high deposition temperature and their density is given by Eq. (8).

B. A phenomenological model for bulk thermal equilibration

The extension of the doping model to explain the present results is rather straightforward. All that is re-

quired is to allow thermal equilibrium to persist in the bulk after deposition, above the equilibration temperature T_E . Below this temperature, the equilibrium is frozen out. In this section, we show that all the experimental results can now be explained phenomenologically. Later we discuss the possible microscopic mechanisms that control the equilibration.

In the temperature range above T_E , the structure is in equilibrium. Thus, according to the defect compensation model, E_F will remain fixed at E_{min} independent of temperature. It is easy to see from Eq. (8) that the value of n_{BT} will be temperature dependent, increasing as the temperature is raised, as is observed by the experiments. As the sample is cooled below T_E , the structure is frozen into a slowly relaxing state. In the frozen state, n_{BT} is greater than its equilibrium value, and is independent of changes in temperature. E_F is no longer required to be at E_{min} since that was based on an assumption of equilibrium. In fact, E_F must move up into the band tail as the temperature decreases in order to satisfy Eq. (8). Thus the main distinction between the two temperature regimes is that above T_E , n_{BT} is temperature dependent and E_F is fixed, whereas below T_E , n_{BT} is constant and E_F becomes temperature dependent.

The bias annealing effects described in Sec. IIF are readily explained with the same equilibration model. Depletion by the bias tends to move the Fermi energy into the gap away from the equilibrium position. Equilibrium is restored by compensating changes in the structure which increase n_{BT} back to its undepleted value, either by decreasing N_{DB} or increasing N_{donor} . When the new equilibrium is frozen in, and the depletion bias is removed, there will be excess n_{BT} , which will undergo slow relaxation, as observed.

The results can be easily modeled with the appropriate density of states distribution $g(E)$. There is still considerable controversy and uncertainty about $g(E)$. Nevertheless, it is probably best known for n -type material and we therefore focus on these data. The density of states shown in Fig. 18 is the same as we have used before,¹² and is essentially that determined by Jackson *et al.*³² The upper part of the conduction band is obtained from inverse photoemission data.^{32,33} For the lower part of the conduction band, we assume an exponential band tail of slope 20 meV⁻¹. The slope is taken from our time-of-flight measurements of electron mobility in undoped samples, using the dispersive transport model of Tiedje and Rose.³⁴ We cannot measure the slope in this way in doped samples, but rather rely on other observations that the drift mobility is similar in undoped and n -type samples.³⁵ The position and shape of the dangling bond band is taken from DLTS data on our samples.³⁶ Other DLTS measurements have a different peak position by up to 0.1 eV.¹⁹ The position of the donor band is constructed to be consistent with the ESR data, which gives the occupancy of the donors and band tail states as a function of doping.²⁶ We assume that the donors have the same low-energy slope as the band tail although the exact shape hardly affects the results. The minimum in the density of states is found by simple extrapolation. Clearly there is uncertainty in the location of the minimum which we esti-

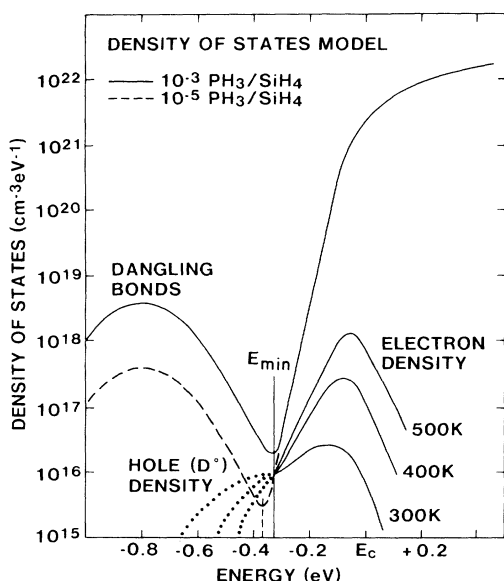


FIG. 18. Model density of states used to calculate the electronic properties. Also shown are the electron and hole (D^0) distributions at different temperatures, assuming the Fermi energy is at E_{\min} .

mate to within ± 50 meV. The position of the mobility edge is assumed to be where the density of states is $2.5 \times 10^{21} \text{ cm}^{-3} \text{ eV}^{-1}$, which is consistent with the photoemission results.³² The density of dangling bonds is set to the value given by many experiments and varies with the doping level. The model in Fig. 18 shows values for two doping levels.

Figure 18 shows the product of $g(E)$ and the Fermi function for three temperatures and for a doping level of $10^{-3} \text{ PH}_3/\text{SiH}_4$. Several points can be noted. First, the electron density increases rapidly above E_{\min} , because of the increase in $g(E)$. Thus the density of shallow states does not depend much on the shape of $g(E)$ near the minimum, although of course it is sensitive to the position of E_F . Second, the results confirm that N_{D^0} is indeed very small compared to n_{BT} , the difference being a factor 10–100, so that N_{D^0} can be neglected to a good approximation. Third, the decrease in n_{BT} with temperature is clearly seen.

The magnitude of n_{BT} also agrees well with the experiments. The calculated temperature dependence (dashed

line) is compared to the experimental results in Fig. 6. In these calculations, we have adjusted E_F to give agreement with the data near 150°C , but there are no other adjustable parameters in the model. The position of E_F is 30 meV above the minimum of $g(E)$, which is within the uncertainty to which $g(E)$ is known. If we had set E_F exactly at E_{\min} , n_{BT} would decrease by about 50%, and the form of the temperature dependence would be virtually unchanged. Thus the modeling confirms that E_F is at least very close to E_{\min} , as we had assumed.

The model also provides a quantitative interpretation of the conductivity data. These results are published in more detail elsewhere and are summarized here.²⁴ In the high-temperature region above T_E , we again set E_F at E_{\min} so the conductivity is given by

$$\sigma = \sigma_0 \exp[-(E_C - E_{\min})/kT]. \quad (10)$$

The value of σ_0 should be Mott's minimum metallic conductivity, with a small correction for the temperature dependence of the band gap, and indeed σ_0 is found to be $\sim 200 \Omega^{-1} \text{ cm}^{-1}$, in good agreement with Mott's value.³⁷ Table I compares the value of $E_C - E_{\min}$ estimated from the model density of states, with the experimentally measured activation energies, for different doping levels. The values are within 50 meV, which is as good agreement as can be expected. The results also indicate that the choice of position of E_C cannot be in error by more than 50 meV.

Below T_E , the Fermi energy is temperature dependent in order to maintain a constant n_{BT} , so that

$$\sigma = \sigma_0 \exp\{-[E_C - E_F(T)]/kT\}. \quad (11)$$

E_F moves up the band tail with decreasing temperature so that

$$E_F = E_F^0 - T\delta(T), \quad (12)$$

where $\delta(T)$ is positive, and would be a constant in the case of a linear temperature dependence. E_F^0 is the limiting position of E_F at zero temperature. Hence

$$\sigma = \sigma_0 \exp[-\delta(T)/k] \exp[-(E_C - E_F^0)/kT]. \quad (13)$$

This well-known "statistical shift" reduces both the apparent activation energy and the conductivity prefactor. If $\delta(T)$ is constant, then the conductivity can be described by a single activation energy, but for other cases there will be curvature in an Arrhenius plot.

The experimental results again agree well with the model. The reduction in the prefactor and the activation

TABLE I. The activation energies for dc conductivity in the two temperature regimes (above and below T_E), showing the agreement between the data and the calculated values derived from the density of states in Fig. 18 and the model described in the text.

[PH ₃]/[SiH ₄]	Conductivity activation energy (eV)			
	$T < T_E$		$T > T_E$	
	Measured	Calc.	Measured	Calc.
10^{-5}	0.21	0.23	0.40	0.37
10^{-4}	0.175		0.34	0.35
10^{-3}	0.16	0.15	0.28	0.33

energy below T_E are as expected. Furthermore, Fig. 19 compares the data and model calculations. The temperature dependence of σ for the low-temperature regime is calculated by numerically integrating Eq. (8), using the density of states in Fig. 18. The freezing temperature was taken to be 130°C as indicated by experiment, and a free-carrier mobility of 15 cm²/V sec was chosen to obtain agreement between experiment and calculation at 300 K for the 10⁻⁵ doped sample. The model gives an activation energy within 20 meV of the experimental value (see Table I) and a prefactor within a factor 4. There is a little more curvature in the model results than in the data, but all three features of the data are well within the uncertainty of $g(E)$.

The excellent agreement between the model calculations and the data lead us to deduce that the phenomenological interpretation of the equilibration in terms of the defect compensation model is correct. Furthermore, the model density of states must also be essentially correct. In the next two sections, we discuss the possible microscopic mechanisms for the equilibration process.

C. Microscopic mechanisms of equilibration

There are several aspects of the results that must be explained by local atomic-scale reactions. First is that equilibration changes the values of $N_{\text{donor}} - N_{\text{DB}}$, increasing this quantity with temperature. We have some experimental evidence that N_{DB} changes, but at present no information about N_{donor} . Second, the equilibration process satisfies Eq. (7), which maintains P_4^+ and D^- states rather than the neutral species. Third, the mechanism must explain the freezing of the defect structure as the temperature is reduced.

Unfortunately, there are a great many microscopic re-

actions that could contribute and there is little experimental information to help identify the primary reactions. At present all we can do is consider the most obvious possibilities. One guide regarding the possible mechanisms comes from the defect compensation model. There it is argued that P_4^+ and D^- states are stable but that P_4^0 states are not. Furthermore, D^0 states are often unstable in undoped α -Si:H and can be removed by annealing. Since the relative concentrations of neutral and charged states of either defect depend on the position of E_F , it is easy to see how the equilibration process determines E_F .

The basic reaction of the doping model given by Eq. (7) is an obvious starting point. In the bulk material, there are at least two mechanisms by which the transformation of a P_3^0 into a P_4^+ and a D^- can occur. One possibility is that a Si—Si bond breaks, with one of the atoms forming a bond to a neighboring P_3 atom creating a P_4 state and the other atom remaining as a dangling bond. A second mechanism is by the motion of hydrogen from a Si—H bond to form a fourth bond to a phosphorus atom, as is indicated schematically in Fig. 20(a).³⁸ We presume that P_4 states are donors irrespective of whether any of the bonds are to hydrogen, but have no information on this point. The second of these mechanisms seems to us the more probable because the rigidity of the fourfold silicon bonding is such that the direction of any one bond cannot move much without incurring a large strain energy. The motion of hydrogen from site to site also allows

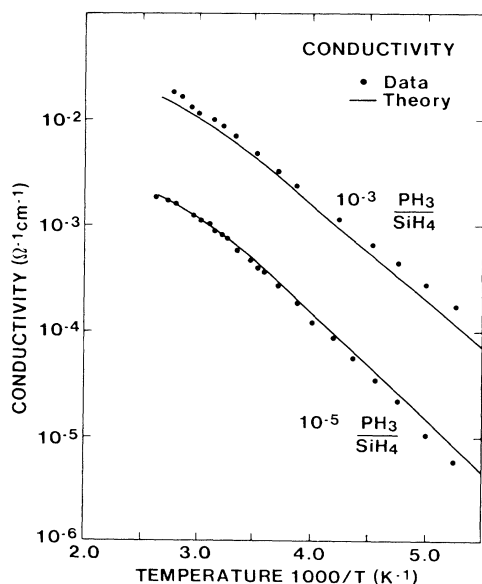


FIG. 19. A comparison of the measured and calculated temperature dependence of dc conductivity in the low-temperature regime for two phosphorus doping concentrations. Details of the calculation are given in the text.

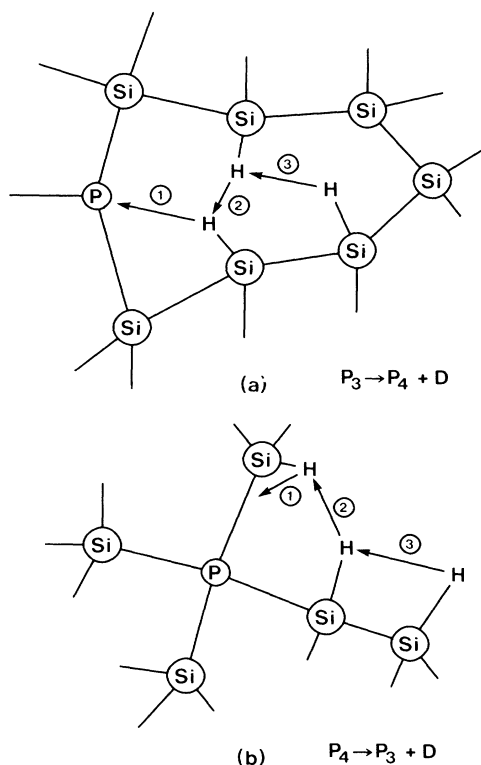


FIG. 20. Examples of possible reactions that change the coordination of phosphorus and the density of dangling bonds through the motion of hydrogen. The numbers indicate the sequence of hops.

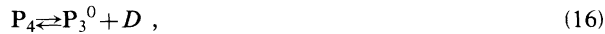
the dangling bond to effectively diffuse away from the P_4^+ , which increases the stability of the structure. Conversely, the opposite reaction requires the D^- to move closer to the P_4^+ in order to revert to a P_3^0 , and here again the motion of hydrogen would facilitate dangling bond diffusion.

According to Eq. (7), the transformation of P_3 states preserves equal densities of both P_4^+ and D^- . Evidently, this reaction cannot explain the increase in n_{BT} which is the difference in the densities of P_4^+ and D^- states. We have previously noted¹¹ that there can be intermediate steps in the reaction described by Eq. (7), for example,



Here, e denotes an electron occupying a conduction-band-tail state. These two reactions provide a general mechanism for separately varying the dangling bond and donor densities at the surface. However, the microscopic mechanism in the bulk is not obvious, since coordination numbers can only be changed in pairs. Thus it is possible to create two dangling bonds either by simply breaking a Si—Si bond, or more likely by inserting a hydrogen into a weak bond, as proposed for the mechanism to explain the Staebler-Wronski effect.⁷ The latter mechanism would obviously allow n_{BT} to vary.

Another process that could change the relative concentration of P_4 and D states is described by



where the P_4 and D states might be neutral or positively charged. For example, if hydrogen were inserted into a P—Si bond from a neighboring site, then Eq. (16) would follow. The schematic illustration in Fig. 20(b) again shows that the dangling bond can diffuse away by hydrogen exchange. This reaction represents a possible mechanism by which neutral donors are removed. The annihilation of neutral dangling bonds could be achieved by reconstruction in pairs to form Si—Si bonds. Again since this can occur only when the two dangling bonds are close, their motion via the diffusion of hydrogen seems to be implied.

We conclude that it is easy to find microscopic bonding mechanisms which are consistent with the equilibration process. It is presently not possible to determine in detail the reactions that dominate the process, which must wait for more experimental information or a better understanding of the energetics of the different processes. We note that Muller *et al.*¹⁸ give a more detailed analysis of the possible reactions. However, it is hard to escape the conclusion that the motion of hydrogen is of central importance to the equilibration mechanism. The same conclusion has been drawn from virtually all studies in which structural changes occur, for example, the annealing of dangling bonds created by light or by particle damage are both associated with the motion of hydrogen.^{7,39} The reason is that hydrogen provides the flexibility to rearrange the bonding structure that is hard to accomplish via the very rigid fourfold coordinated silicon network. The next section expands on the idea that hydrogen motion is

important by proposing a specific model to describe that motion.

D. The hydrogen-glass model

The equilibration process has been shown to have the following properties.

- (i) A metastable equilibrium at high temperature.
- (ii) A thermally activated equilibration time.
- (iii) A slowly relaxing frozen-in state at low temperatures.

We point out that these are also the characteristic properties of a glass. The glass transition temperature is the demarcation between the metastable equilibrium phase and the frozen-in state of a glass. The glass transition is determined kinetically, being a balance between the cooling or heating rate and the thermally activated equilibration time. A characteristic property of a glass is a change in the temperature dependence of structurally related quantities at the glass transition temperature. The kink in the conductivity data and the change in n_{BT} at the equilibration temperature are qualitatively similar to the behavior observed in conventional glasses. In view of the similarities, it is pertinent to ask if doped α -Si:H can be considered as a glass. We have already argued that hydrogen is most probably involved in the microscopic process of equilibration. Based on this idea, we propose the following model.

The silicon random network, being fourfold coordinated, is very rigid; it seems extremely unlikely that it could have glassy properties. Furthermore, the fact that α -Si cannot be formed by cooling from the melt appears to rule it out as a glass. On the other hand, the bonded hydrogen is more mobile, and is known to diffuse at relatively low temperatures. We therefore propose that the network of bonded hydrogen can be considered as a glass. Thus the α -Si:H network can be divided into two interconnecting submatrices, one of which is rigid and the other glassy. Although the two submatrices are highly interlocking, we suppose that they are sufficiently distinct to be described as separate entities. We draw the analogy with a superionic conductor which has a rigid sublattice and a separate sublattice which melts upon heating. However, in the present case, instead of melting, the bonded hydrogen passes through a glass transition.

In order for the H-glass model to be valid, two conditions should be satisfied. First, we must show that the equilibration is indeed due to the motion of hydrogen. Second, all the hydrogen must be available for the equilibration process rather than a particular small subset of hydrogen located at some special sites. If both conditions are fulfilled, then above T_E the entire hydrogen submatrix must be in metastable equilibrium, freezing out of equilibrium below T_E . These properties provide the necessary elements of glassy behavior.

Although we do not yet have complete proof of these two requirements for a glass, the evidence suggests that the H-glass is a correct description. In the preceding section, we argued that it is difficult to find any microscopic

model for the equilibration that does not involve the motion of hydrogen. In order to explore further the role of hydrogen motion, we have measured the temperature dependence of its diffusion. The measurements are made on samples that contain a thin deuterated layer sandwiched between layers of doped *a*-Si:H. The deuterium profile is obtained by secondary-ion mass spectroscopy (SIMS), with the samples being annealed to temperatures between 150°C and 300°C for varying times. The technique is that described by Carlson and Magee who found that the diffusion coefficient, D , in undoped *a*-Si:H had an activation energy of about 1.5 eV.⁴⁰

Figure 21 shows our data on boron and phosphorus doped *a*-Si:H. The gas-phase doping level in each case is 10^{-3} . The most striking result we find is that the hydrogen diffusion coefficient is much larger in the doped samples compared to the undoped, and is larger in *p*-type material compared to *n* type. Our own undoped samples are consistent with the more complete data of Carlson and Magee.⁴⁰ Furthermore, we find that compensated *a*-Si:H has a low diffusion coefficient, similar to that of undoped *a*-Si:H, so that the high value in *p*-type *a*-Si:H is not simply due to the presence of boron. An interesting aspect of our data is that the difference between boron and phosphorus doping matches our observation that T_E is lower in *p*-type samples than in *n* type.

We next relate the diffusion coefficient to the microscopic motion of the hydrogen. Assuming that the diffusion can be described by a series of discrete hops from site to site with separation a , the coefficient is given by

$$D = a^2 p_H, \quad (17)$$

where p_H is the average rate at which each hydrogen hops. Hence the total hop rate is

$$R_H = N_H p_H = N_H D / a^2, \quad (18)$$

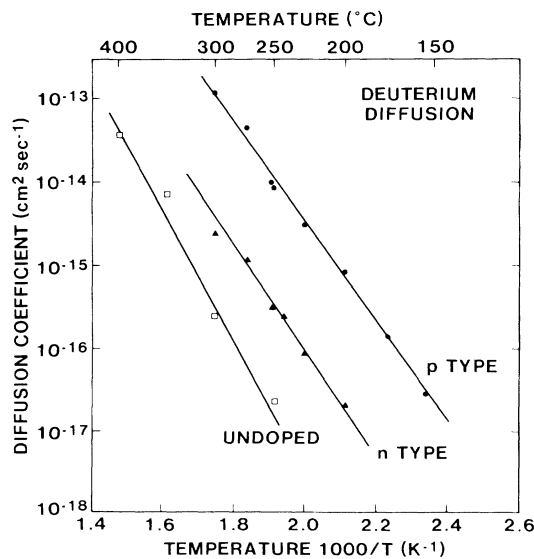


FIG. 21. Plot of the temperature dependence of the deuterium diffusion coefficient in undoped, *n*-type and *p*-type *a*-Si:H. The undoped data is taken from Carlson and Magee (Ref. 40).

where N_H is the hydrogen concentration. If we assume $a = 5 \text{ \AA}$ and $N_H = 5 \times 10^{21} \text{ cm}^{-3}$, then at a diffusion coefficient of $10^{-18} \text{ cm}^2 \text{ sec}^{-1}$, the total hop rate is $2 \times 10^{18} \text{ cm}^{-3} \text{ sec}^{-1}$. The relevance of these numbers will soon become clear.

The detailed mechanism of hydrogen diffusion has not been clearly established. However, since essentially all the hydrogen is bonded to Si atoms, these must be the hopping sites. We suggest that in order for hydrogen to move, there must be an unterminated silicon bond near by for the hydrogen to hop to, so that the diffusion coefficient will be proportional to the dangling bond density. Since doped *a*-Si:H contains a larger density of dangling bonds than undoped *a*-Si:H, the larger values of D in Fig. 21 can be readily understood, as can the low values of D in compensated *a*-Si:H, which is known to have a low dangling bond density.²⁸ Whatever the detailed mechanism of diffusion, it is clear that when hydrogen is released from one site, a dangling bond is created, and when the H atom lands at an unterminated silicon atom, a dangling bond is annihilated. Hydrogen diffusion must therefore influence the electronic defects.

The rate at which the dangling bonds diffuse by this mechanism is surprisingly large. At a doping level of 10^{-3} , as in the data of Fig. 21, the dangling bond density is 10^{18} cm^{-3} . From Eq. (18), we found that for a diffusion coefficient of only $10^{-18} \text{ cm}^2 \text{ sec}^{-1}$, the hop rate corresponded to the motion of that many dangling bonds each second. The temperatures corresponding to $D = 10^{-18} \text{ cm}^2 \text{ sec}^{-1}$, obtained by extrapolating the data in Fig. 21, are 110°C for *p* type and 160°C for *n* type *a*-Si:H. Thus the diffusion of hydrogen is sufficient to rapidly move dangling bonds well below the deposition temperature and close to the measured equilibration temperature.

Therefore, over a substantial temperature range we must view the defects in doped *a*-Si:H not as fixed entities, but as states that move rapidly within the material.

In attempting to validate the H-glass model, another approach is to consider the relation between diffusion and the viscosity of a glass. The glass transition of a conventional glass is generally considered to occur at a viscosity of 10^{13} P (dyn sec/cm²). In a covalent solid such as SiO₂, viscous flow is associated with bond rearrangements via a mechanism that is clearly related to the self-diffusion of the elements of the glass. The viscosity η is related to diffusion by the Stokes-Einstein relation

$$\eta D = kT / 6\pi R, \quad (19)$$

where R is the effective radius of the self-diffusing species. When T is the equilibration temperature, $\sim 100^\circ\text{C}$, and $R = 3 \text{ \AA}$, Eq. (19) yields a value of $\sim 10^{-7}$ dyn. This value is also found empirically by comparing materials in which both η and D are known.⁴¹ The diffusion coefficient associated with the glass transition temperature is therefore of order $10^{-20} \text{ cm}^2 \text{ sec}^{-1}$. Again, from the data of Fig. 21, the corresponding extrapolated temperatures are 130°C and 80°C for *n*- and *p*-type samples, respectively, in excellent agreement with the observed equilibration temperatures.

The measurements of diffusion reflect the motion of all (or most of) the hydrogen in the film. The fact that the

diffusion coefficients are consistent with equilibration occurring at the observed temperatures, implies that all the hydrogen is available for the equilibration process. Since the value of T_E in *n*-type samples of 130°C corresponds to an equilibration time of 10 min, and a hydrogen diffusion coefficient of $\sim 10^{-20}$ cm²sec⁻¹, we estimate that each dangling bond makes ~ 5 hops before equilibrating, and about 0.1% of the hydrogen has moved.

The above discussion makes no attempt to distinguish between the clustered and dilute phases of bonded hydrogen that have been identified by nuclear magnetic resonance (NMR).⁴² Our SIMS data show no distinction in the diffusion coefficients, and we cannot tell whether both phases contribute to the equilibration process which must wait for further studies. NMR measurements find that annealing an undoped sample to 200°C results in a small redistribution of the hydrogen within the two phases.⁴² The change coincides with a reduction in the dangling bond density, again suggesting that hydrogen motion is the mechanism by which the density of states changes.

Based on the above arguments, we believe that the H-glass model is an appropriate description of the structure. Within this description we equate the equilibration temperature T_E with the glass transition temperature. To our knowledge this is the first example of a material which comprises two distinct atomic substructures, only one of which has glassy properties. (However, a spin glass might be a magnetic analogy.) It is interesting to note that our results have several phenomenological similarities to the properties of conventional glasses. For example, the time-dependent relaxation below T_G is generally nonexponential, as we observe, and is often fitted to a stretched exponential function $\exp[-(t/\tau)^\beta]$.⁴¹ This function also gives a reasonable fit to our data. The activation energy for relaxation typically drops by a factor 2 below T_G , and again the same behavior is observed in the present case. These characteristic properties are not fully understood in glasses.

IV. DISCUSSION

A. Undoped *a*-Si:H and other equilibration models

So far our experiments and analysis have focused solely on doped *a*-Si:H, because these materials show the clearest evidence of equilibration. It is of course pertinent to ask whether undoped *a*-Si:H can also be described in a similar way. This possibility was first proposed by Smith and Wagner,¹⁵ who focused on the dangling bond density. If the energy to form a dangling bond is E , then in equilibrium their density should be proportional to $\exp(-E/kT)$. Unfortunately, the energy E is not known accurately either by experiment or calculation. Smith and Wagner instead used information on the creation of dangling bonds by prolonged illumination. The current model for the Staebler-Wronski effect is that the energy released by the nonradiative recombination of an electron and hole creates the excess dangling bonds, and the creation rate has been measured by experiment.⁷ Smith and Wagner argue that thermally generated electrons and holes will produce dan-

gling bonds by the same mechanism, and from the known rates they deduce that at a deposition temperature of 500 K, the equilibrium density of dangling bonds should be about 10^{15} cm⁻³. Since the observed density is roughly of this magnitude, they proposed that in the best undoped *a*-Si:H films, the equilibrium dangling bond density is frozen in near, but below, the deposition temperature. More recently, they have reported that fast quenching results in an increased dangling bond density, which is clear experimental evidence for the equilibration.¹⁶

In contrast, Muller *et al.*¹⁸ conclude that the dangling bonds in undoped *a*-Si:H are not in equilibrium. They also calculate the density from known parameters, but in this case they use the dangling bond densities in doped samples, assuming equilibrium as in the defect-compensation model. Their model results in an estimated 10^{13} – 10^{14} cm⁻³ dangling bonds at the deposition temperature in undoped material, which is significantly below the observed value. They therefore conclude that the dangling bonds do not equilibrate during deposition, and attribute their presence to local strain in the Si network. Clearly these two models need to be reconciled.

A different model has been proposed by Bar-Yam *et al.*¹⁷ They suggest that the equilibration is much more extensive than in our description, involving the complete Si network. In their model, the band-tail density of states is also determined by thermal equilibrium. They argue that the excess energy to produce a state at energy E from the band edge is of order E , so that the density of states varies as $\exp(-E/kT_E)$. Thus the observed exponential band tails are easily explained. The different slopes of the valence and conduction band are accounted for by an *ad hoc* correction to the energy E . In their model the dangling bonds are also determined by equilibrium. Their model includes negative correlation energy defects which are based on their previous theoretical calculations, but which seems to be at odds with the experimental information, which has always found a positive correlation energy.

Clearly, the extent of the equilibration in either doped or undoped *a*-Si:H remains to be determined more precisely by experiment. On the one hand, it is possible that equilibration is a rather restricted process involving a relatively small density of states ($\sim 10^{17}$ cm⁻³) because this is the extent of the observable changes. At the other extreme is the suggestion that the entire Si network equilibrates (though presumably not to the extent of forming the crystalline phase). We take the intermediate view, as discussed above, that equilibration in doped *a*-Si:H involves all or most of the bonded hydrogen, but is probably not applicable to the Si network. Since our experimental data are on doped samples, and our interpretation is closely tied to the doping process, it is hard to relate our results to undoped *a*-Si:H. One point can be made, however. We argued that the equilibration temperature is associated with a hydrogen diffusion coefficient of $\sim 10^{-20}$ cm²sec⁻¹. Extrapolation of the data in Fig. 21 therefore suggests that undoped *a*-Si:H equilibrates at 190°–200°C. Since the deposition occurs just above this temperature, equilibration seems a viable proposition, but evidently occurs at a higher temperature than in the doped samples.

B. Relation to the deposition process

In the Introduction it was noted that in the past *a*-Si:H has been viewed as a nonequilibrium material whose structure and properties are determined by the deposition process. As we have discussed, such a view can no longer be held. It is interesting that notions about the plasma deposition have recently been changing in a way that may relate closely to the present experiments. The work of Tsai *et al.*⁴³ has shown that there are two regimes of deposition in *a*-Si:H: one is termed physical vapor deposition (PVD) and the other chemical vapor deposition (CVD). The distinction is that in a PVD process, the atoms or radicals impinge on the surface from the gas, and essentially remain where they arrive. In contrast, CVD deposition is controlled by a chemical reaction at the growing surface. An ideal CVD process occurs without the plasma, and is driven simply by the thermal decomposition of the gas. The plasma is viewed as a perturbation of the gas, providing a source of radicals that can undergo a CVD reaction at the surface. The different mechanisms have been associated with different gas radicals. In the CVD process, deposition is believed to be primarily from SiH₃, which has a low sticking coefficient and relies on a hydrogen elimination step for film growth. In PVD the radicals are more reactive, and immediately bond to the surface.⁴⁴ The PVD process is clearly nonequilibrium, whereas the ideal CVD deposition is a thermal equilibrium process.

Tsai *et al.* are able to distinguish between the two types of deposition by the way in which a deep trench cut into a substrate is coated with *a*-Si:H. In cross section, the PVD deposition give a well-defined cusped structure at the bottom of the trench, due to shadowing by the trench walls, whereas the CVD process gives a conformal coating. They find that when *a*-Si:H is deposited at high rf power, and with SiH₄ diluted in an inert gas, the growth mechanism is PVD. Furthermore, the columnar microstructure of the material is associated with this type of growth. On the other hand, low-power deposition without dilution give almost conformal coatings characteristic of a predominantly CVD mechanism. These conditions yield good electronic properties and correspond to all the samples studied here.

It seems plausible that there is a direct relation between the type of deposition and the equilibration of bulk *a*-Si:H. We speculate that the PVD process probably does not allow a bulk equilibrium because the deposition itself is far from equilibrium. The observation that *a*-Si:H can be grown by PVD with a large defect density which cannot be removed by annealing, clearly indicates that the defects are not equilibrated. On the other hand, in CVD the surface grows under conditions close to equilibrium, and the equilibration may persist into the bulk. This model provides a direct explanation of why the lowest defect density *a*-Si:H is obtained only with CVD deposition. It would clearly be of interest to investigate the doping properties of PVD grown material.

C. Other experiments

There are several other experiments, apart from those described in Sec. II in which equilibrium plays an impor-

tant role. We first discuss some past experiments that can be interpreted using our new understanding. Ast and Brodsky⁴⁵ observed the quench rate dependence in the dc conductivity, with data that are comparable to ours, in that faster quenching resulted in higher conductivity. They observed the effect in both *n*-type and undoped *a*-Si:H, which is therefore some further evidence of equilibration in undoped samples.

Another measurement that can now be understood more clearly is that of Lang *et al.*⁴⁶ They observed a metastable, field-induced doping effect in which the donor concentration appeared to increase with temperature above 150°C. Their experiment actually measures the same shallow state density n_{BT} as ours, so their observations are in good agreement with ours. Since in their experiment n_{BT} can be measured at an elevated temperature without having to quench in the value, it may provide a more direct measure of $n_{BT}(T)$. However, the experiment is complicated by the applied bias to the sample, which introduces other effects, as described in Sec. IIF.

In other DLTS studies, Crandall has reported a defect with unusual properties.⁴⁷ The capture cross section of this defect is activated with about the same energy as for release of electrons from the trap. Both energies are about 1 eV, and the DLTS is observed above 100°C. Crandall interprets the data in terms of a shallow state with a very large barrier surrounding it. The experimental indication for the activated cross section is that the trap cannot be filled by a voltage pulse except at high temperature. We believe that the results may be explained by thermal equilibration of the structure, and that the activated capture in fact reflects the temperature dependent change in the structure. The fact that the DLTS signal begins to be observed at 130°C, and that the activation energy is similar to that of the equilibration time, strongly indicates a connection between the two results.

We have shown that a depletion bias will enhance n_{BT} , and so similarly, an accumulation bias should reduce it. We have no direct experimental verification of this prediction. However, it is known from other experiments that current injection in *p-i-p* structures increases the defect density which will of course reduce n_{BT} .⁴⁸ From our results, we can understand why the effect is observed only for *p*-type samples at room temperature. The response time is too slow in *n*-type samples at room temperature. We predict that similar results would be observed in *n-i-n* structures if the temperature during current injection were ~70°C. An improvement of solar-cell performance is observed after annealing in reverse bias.⁴⁹ At present, it is unclear whether the main changes originate in the doped contact layers or the undoped film. In either case an improvement in properties through equilibration of the structure is expected.

A very different situation in which slow relaxation effects are observed is in the studies of surface adsorbates.⁵⁰ Tanelian finds that exposure of *a*-Si:H to H₂O, NH₃, or other gasses results in conductivity transients extending for several hours, and that both a slow and a fast process can be identified. The slow process was postulated to be a chemical reaction mediated by the presence of the surface oxide. Our results suggest an alternative model, that the

slow process may be the bulk equilibration after the adsorbed gas has changed the Fermi energy at the surface. The observed time constant is consistent with equilibration for p -type a -Si:H but is faster than we find in n -type material. At present we cannot determine whether the equilibration process is a significant contribution to the adsorbate effects.

Finally we suggest that thermal equilibration processes may play an important role in the persistent photoconductivity effect (PPC) that is observed in doping modulated superlattices.⁵¹ These structures consist of alternatively doped n -type and p -type layers. A brief light exposure enhances the dark conductivity by many orders of magnitude. This excess conductivity requires many days to decay at room temperature, but can be removed by annealing above 130°C. The photoexcited electron-hole pairs are spatially separated during illumination with the electrons moving into the n layers and holes into the p layers. The dielectric relaxation time to dissipate the stored charge is too short to account for the long relaxation times, and so most models of PPC involve special traps. As discussed above, the loss of excess carriers via thermal relaxation of the electronic states is much more rapid in p -type a -Si:H compared to n type. Those holes lost through equilibration would be unable to recombine with the spatially separated electrons in the n layer. The long decay time for PPC is then explained by the slow relaxation of the structure, and the annealing temperature reflects the equilibration of the material. Further details of this model will be published separately.⁵²

V. CONCLUSIONS

The main conclusions of the paper are as follows.

(1) There is extensive evidence that a substantial part of the atomic structure is in thermal equilibrium above $\sim 130^\circ\text{C}$ in n -type, and 80°C in p -type a -Si:H. Below these temperatures the time to reach equilibrium is very long and the structure is frozen into a slowly relaxing state. The equilibration time, $\tau_E(T)$, has an activation energy that increases from 0.65 eV at low temperatures up

to ~ 1.0 eV above T_E .

(2) The thermal equilibrium is readily observable through changes in the electronic properties. In particular the density of electrons or holes occupying band tail states increases above T_E , and there is a change of slope in the temperature dependence of the dc conductivity.

(3) The equilibrium structure can be controlled by an external bias, so that it is possible to modify the density of carriers that are frozen in.

(4) The defect-compensation model of doping provides a phenomenological model to describe the results. The thermal equilibrium is maintained by changes in the density of dangling bonds and donors or acceptors. We argue that the Fermi energy is held between the band tail and the dangling bonds in equilibrium, but will move up the band tail below T_E .

(5) A quantitative fit to the data is obtained using the known density of states distribution. In particular, we can account for the temperature dependence of the density of shallow states, and fit the conductivity data over the entire temperature range.

(6) The microscopic mechanisms of equilibration are discussed with the conclusion that the motion of hydrogen from site to site, and its insertion into Si—Si bonds, is probably the dominant mechanism.

(7) Based on our observations, we propose that the bonded hydrogen can be described as a structurally separate submatrix which has glassy properties, whereas the Si matrix is rigid. New hydrogen diffusion data are presented to support this model.

ACKNOWLEDGMENTS

We are grateful to W. Jackson and M. Stutzmann for helpful discussions, to Y. Bar-Yam and Z. Smith for copies of their unpublished work, and to R. Thompson and J. Zesch for technical assistance. We thank M. Stutzmann for the ESR measurements. The work is supported by the Solar Energy Research Institute (Golden, CO).

¹N. F. Mott and E. A. Davis, *Electronic Processes in Non-crystalline Materials* (Clarendon, Oxford, 1979).

²M. H. Brodsky and R. S. Title, *Phys. Rev. Lett.* **23**, 581 (1969).

³R. A. Street, J. C. Knights, and D. K. Biegelsen, *Phys. Rev. B* **18**, 1880 (1978).

⁴J. C. Knights and R. A. Lujan, *Appl. Phys. Lett.* **35**, 244 (1979).

⁵See, for example, J. Stuke, in *Proceedings of the 7th International Conference on Amorphous and Liquid Semiconductors*, edited by W. E. Spear, (CICL, Edinburgh, 1977), p. 406.

⁶D. L. Staebler and C. R. Wronski, *Appl. Phys. Lett.* **31**, 292 (1977).

⁷M. Stutzmann, W. B. Jackson, and C. C. Tsai, *Phys. Rev. B* **32**, 23 (1985).

⁸G. Lucovsky, *Phys. Rev. B* **6**, 1480 (1972).

⁹M. Abkowitz and D. M. Pai, *Phys. Rev. B* **18**, 1741 (1978); M. Abkowitz and R. C. Enck, *J. Non-Cryst. Solids*, **35& 36**, 831

(1980).

¹⁰R. A. Street, *Phys. Rev. Lett.* **49**, 1187 (1982).

¹¹R. A. Street, D. K. Biegelsen, W. B. Jackson, N. M. Johnson, and M. Stutzmann, *Philos. Mag. B* **52**, 235 (1985).

¹²R. A. Street, *J. Non-Cryst. Solids* **77& 78**, 1 (1985).

¹³A square root dependence on gas concentration is always observed. However in some cases (e.g., As doping) the dependence on the solid phase concentration is different. The origin of this behavior is unclear, and is discussed by M. Stutzmann, *Philos. Mag. B* **53**, L15 (1986).

¹⁴R. A. Street, J. Kakalios, and T. M. Hayes, *Phys. Rev. B* **34**, 3030 (1986).

¹⁵Z. Smith and S. Wagner, *Phys. Rev. B* **32**, 5510 (1985).

¹⁶Z. Smith, S. Aljishi, D. Slobodin, V. Chu, S. Wagner, P. M. Lenahan, R. R. Arya, and M. S. Bennett, *Phys. Rev. Lett.* **57**, 2450 (1986).

¹⁷Y. Bar-Yam, D. Adler, and J. D. Joannopoulos, *Phys. Rev.*

- Lett. **57**, 467 (1986).
- ¹⁸G. Muller, S. Kalbitzer, and H. Mannsperger, Appl. Phys. A **39**, 243 (1986).
- ¹⁹D. V. Lang, J. D. Cohen, and J. P. Harbison, Phys. Rev. B **25**, 5285 (1982).
- ²⁰R. A. Street, Philos. Mag. B **50**, L19 (1984).
- ²¹R. A. Street, M. J. Thompson, and N. M. Johnson, Philos. Mag. B **51**, 1 (1985).
- ²²R. A. Street, Phys. Rev. B **32**, 3910 (1985).
- ²³M. Stutzmann, Philos. Mag. (to be published).
- ²⁴J. Kakalios and R. A. Street, Phys. Rev. B **34** 6014 (1986).
- ²⁵R. A. Street and D. K. Biegelsen, Solid State Commun. **33**, 1159 (1980).
- ²⁶M. Stutzmann and R. A. Street, Phys. Rev. Lett. **54**, 1836 (1985).
- ²⁷M. Stutzmann, D. K. Biegelsen, and R. A. Street (unpublished).
- ²⁸R. A. Street, D. K. Biegelsen, and J. C. Knights, Phys. Rev. B **24**, 969 (1981).
- ²⁹R. A. Street and J. Kakalios, Philos. Mag. B **54**, L21 (1986).
- ³⁰W. B. Jackson and N. M. Amer, Phys. Rev. B **25**, 5559 (1982).
- ³¹C. R. Wronski, B. Abeles, T. Tiedje, and G. D. Cody, Solid State Commun. **44**, 1423 (1982).
- ³²W. B. Jackson, S. M. Kelso, C. C. Tsai, J. W. Allen, and S.-J. Oh, Phys. Rev. B **31**, 5187 (1985).
- ³³W. B. Jackson, S.-J. Oh, C. C. Tsai, and J. W. Allen, Phys. Rev. Lett. **53**, 1481 (1984).
- ³⁴T. Tiedje and A. Rose, Solid State Commun. **37**, 49 (1980).
- ³⁵W. Daohuai and C. Ruguany, Solid State Commun. **54**, 295 (1985).
- ³⁶N. M. Johnson, Appl. Phys. Lett. **42**, 981 (1983).
- ³⁷N. F. Mott, Adv. Phys. **34**, 329 (1985).
- ³⁸The reactions discussed here are similar to those considered in connection with the Staebler-Wronski effect in doped *a*-Si:H by W. B. Jackson, M. Stutzmann, and C. C. Tsai, Solar Cells (in press).
- ³⁹R. A. Street, D. K. Biegelsen, and J. Stuke, Philos. Mag. B **40**, 451 (1979).
- ⁴⁰D. E. Carlson and C. W. Magee, Appl. Phys. Lett. **33**, 81 (1978).
- ⁴¹See, for example, *Amorphous Materials*, edited by R. W. Douglas and B. Ellis (Wiley-Interscience, New York, 1972).
- ⁴²J. A. Reimer, R. W. Vaughan, and J. C. Knights, Solid State Commun. **37**, 161 (1981).
- ⁴³C. C. Tsai, J. C. Knights, G. Chang, and B. Wacker, J. Appl. Phys. **59**, 2998 (1986).
- ⁴⁴A. Gallagher, MRS Proc. **70**, 3 (1986).
- ⁴⁵D. G. Ast and M. H. Brodsky, in *Proceedings of the 14th International Conference on the Physics of Semiconductors*, Inst. Phys. Conf. Ser. No. 43, edited by B. L. H. Wilson (IOP, Bristol, 1979), p. 1159.
- ⁴⁶D. V. Lang, J. D. Cohen, and J. P. Harbison, Phys. Rev. Lett. **48**, 421 (1982).
- ⁴⁷R. S. Crandall, Phys. Rev. B **24**, 7457 (1981).
- ⁴⁸W. Kruhler, H. Pfeleiderer, R. Plattner, and W. Stetter, in *Proceedings of the International Topical Conference on Optical Effects in Amorphous Semiconductors*, AIP Conf. Proc. No. 120 (AIP, New York, 1984), p. 311.
- ⁴⁹G. A. Swartz, Appl. Phys. Lett. **44**, 697 (1984).
- ⁵⁰M. Tanelian, Philos. Mag. B **45**, 435 (1982).
- ⁵¹J. Kakalios and H. Fritzsche, Phys. Rev. Lett. **53**, 1602 (1984).
- ⁵²J. Kakalios (unpublished).